Supporting information

A universal and accurate LPMI-calculating-method for mismatch in heterogeneous ice nucleation

Qiyuan Deng[1,2], Hong Wang[1,2], Xun Zhu[1,2], Junjun Wu[1,2], Yudong Ding[1,2], Rong Chen[1,2], Qiang Liao[1,2]*

[1] Key Laboratory of Low-grade Energy Utilization Technologies and Systems, Ministry of Education, Chongqing University, Chongqing 400030, China.

[2]Institute of Engineering Thermophysics, School of energy and power engineering, Chongqing University, Chongqing 400030, China

*Corresponding author. Tel.: 0086-23-65102474; fax: 0086-23-65102474; e-mail: lqzx@cqu.edu.cn

- **Supporting Tables S1-S3**
- **Supporting Figures S1-S**
- **Reference**

Experimental Section

Table S1. The definitions of the mismatch δ

Reference	Parameter	δ
David and Bernard [1] Martin and Angelos[2] Liu and Huang[3]	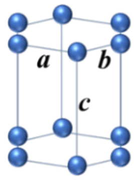	$\delta_1 = \frac{a_i - a_s}{a_i}$
Purppacher[4]	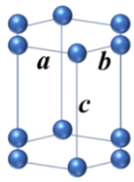	$\delta_2 = \frac{na_n - ma_i}{ma_i}$
Abhishek and Patey[5]	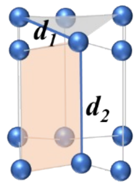	$\delta_{2D} = \frac{\lvert d_i - d_s \rvert}{d_i}$
This investigation	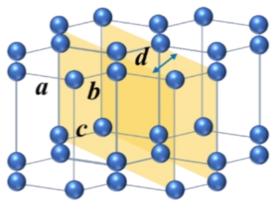	$\delta_d = 2(d_i - d_s)/(d_i + d_s)$

The δ measures the relative size of the lattice constants of the materials used compared to those of the substrate material. For heterogenous ice nucleation, δ denotes the difference in lattice constants of ice and substrate. For δ_1 and δ_2, a is the lattice parameter. For δ_{2D}, d refers distances between two adjacent and congener atoms on the same plane for ice and substrate. For δ_d, d refers the interplanar spacing of the crystal panel. The subscripts s and i are substrate and ice, respectively.

Table S2. Unit cell parameters for crystal structures

Crystal	**Unit cell**	**a (Å)**	**b (Å)**	**c (Å)**	**α (°)**	**β (°)**	**γ (°)**
Ice [6, 7]	Hexagonal	4.506	4.506	7.346	90	90	120
α-Al_2O_3 [8]	Hexagonal	4.75	4.75	12.98	90	90	120
Silicon [9]	Cubic	5.43	5.43	5.43	90	90	90
β-AgI [10]	Hexagonal	4.6	4.6	7.51	90	90	120
PbI_2 [11]	Hexagonal	4.56	4.56	13.97	90	90	120
Gibbsite [12]	Monoclinic	8.69	5.08	9.74	90	90.54	90
Kaolinite [13]	Triclinic	5.15	8.94	7.39	91.93	105.05	89.8
Mica [14]	Monoclinic	5.19	9.03	20.11	90	95.782	90
Hematite [15]	Hexagonal	5.03	5.03	13.75	90	90	120
Boehmite [16]	Orthorhombic	2.85	12.12	3.74	90	90	90
AsI [5]	Hexagonal	4.506	4.506	12.98	90	90	120
AsH [5]	Hexagonal	5.03	5.03	13.75	90	90	120
HsI [5]	Hexagonal	4.506	4.506	13.75	90	90	120

AsI, AaH, and HsI are imitated crystal structures. AsI refers to scaling α-Al_2O_3 to the ice basal plane. AsH refers to scaling α-Al_2O_3 to hematite in the basal plane. HsI refers to scaling hematite to ice (HsI), reducing mismatch to zero for the basal plane

Table S3 the potential for water molecules and temperature

Surface label	Potential for water molecules	T (K)	Water-substrate interaction	Ensembles	Number of molecules
β-AgI [5, 17]	TIP4P/Ice Six-site	230 240	CLAYFF	NPT	1350
Kaolinite [5, 18]	TIP4P/Ice Six-site	230 240	CLAYFF	NPT	1450
Mica [5, 19]	TIP4P/Ice	230	CLAYFF	NPT	6630
PbI_2 [5]	TIP4P/Ice Six-site	230 240	CLAYFF	NPT	1350
Gibbsite [5, 20]	TIP4P/Ice Six-site	230 240	CLAYFF	NPT	1000
Hematite [5, 21]	TIP4P/Ice Six-site	230 240	CLAYFF	NPT	1600
Boehmite [5]	TIP4P/Ice	230	CLAYFF	NPT	1670
AsI [5]	TIP4P/Ice	230	LJ	NPT	1280
AsH [5]	TIP4P/Ice	230	LJ	NPT	1445
HsI [5]	TIP4P/Ice	230	LJ	NPT	1130

Table S4. The freezing delay time in MD simulation

Surface label	Kaolinite[18]	KaonoSi [5]	β-AgI [17]	PbI_2 [5]	α-Al_2O_3 [8]	AsI [5]	AsI(Fe) [5]	HsI [5]	HsI(Fe) [5]
Time (ns)	400	430	80	60	520	360	310	500	250

KaoniSi is produced by Kaolinite removing a layer of Si atoms. AsI,and HsI are imitated crystal structures. Scaling α-Al_2O_3 to hematite (referred to as AsH) increases the mismatch for the basal plane. Scaling hematite to ice (referred to as HsI) eliminates the mismatch on the basal plane. AsI(Fe) and HsI(Fe) are AsI and HsI using Fe LJ forcefield for water-substrate interaction.

Materials and methods in experiment

The experiment system is shown in **Figure S1**. The semiconductor cooler (Ruipu China) is utilized to cool and maintain the substrate at a specific temperature. The plexiglass chamber on the cooler is used to maintain the relative humidity of the freezing environment. The temperature is measured by the thermocouples (Omega USA) and data logger (Agilent USA). The charge-coupled device (CCD) camera (Navitar USA) captures and records the freezing process at 25 fps (frames per second). The experimental steps are as follows.

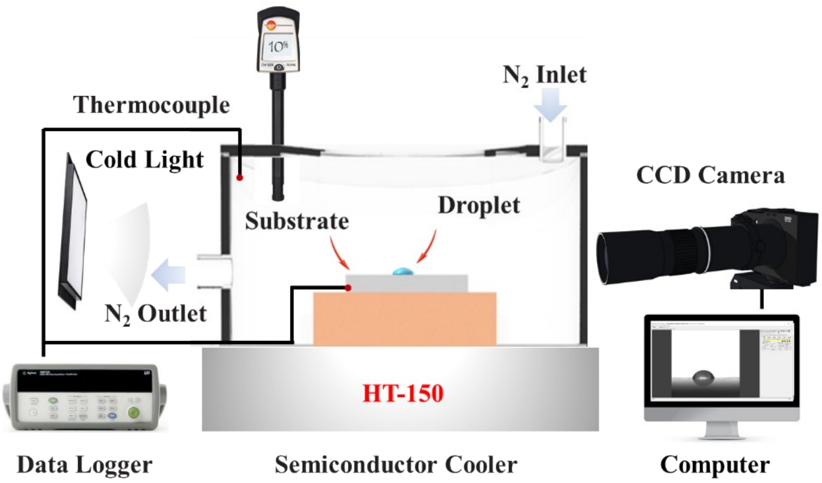

Figure S1. Schematic diagram of the experimental system

10 μL droplets were pipetted onto the substrate by a pipette. Subsequently, N_2 was introduced through the gas inlet of the plexiglass cavity until the relative humidity inside the chamber was below 10%. The relative humidity in the chamber was measured by a hygrometer. Cool the substrate to the target temperature at a cooling rate of 2.8 °C/min. However, for individual droplets, freezing is a random event. Thus, more than 10 freezing experiments were performed on the same substrate. Wherein the

monocrystalline silicon wafers (with Miller index of (100), (110) and (111)) and α-Al_2O_3 flakes (with Miller index of M-plane $(10\bar{1}0)$, A-plane $(11\bar{2}0)$ and C-plane (0001)) were selected as heterogenous nucleation substrates. The thickness of silicon wafer and α-Al_2O_3 flake are 500 μm ±10 μm and 430 μm ±10 μm, respectively (Suzhou Research Materials Microtech Co., Ltd, China). The surfaces of the substrates were prime polished. Before experiments, the surface properties should be characterized. The wettability was observed on an optical contact-angle goniometer (Xuanyi, China). Surface morphology was observed with a scanning electronic microscope (SEM, HITACHI, Japan), and the roughness was measured using an atomic force microscope (AFM, Asylum, USA). The contact angle of 5 μL water droplet was measured as shown in **Figure S2**. Moreover, the SEM and AFM of the substrate surface morphology are shown in **Figure S2**. The AFM measurement (**Figure S3**) indicates that R_a of the substrates is located at 400-600 pm, which is an order of magnitude smaller than the critical nucleation radius R_c (4-11 nm) at the experimental subcooling, namely $R_a < R_c$. The interfacial correlation factor $f(m,x)$ in the heterogenous nucleation can be treated as $f(m,x) = (2-3m+m^3)/4$ [22, 23]. Therefore, interfacial correlation factor f is primarily influenced by m. In summary, the effect of heterogeneous nucleation in our experiment depends on the free energy differences between water and the crystal phase of the substrate, namely, m in f, which is determined by the interaction strength and the structure match[22]. The interaction strength between the same materials can be regarded as identical. Different Miller indices result in different crystal plane structures in contact with water. This study mainly compares the freezing delay times of droplets on silicon wafers and α-Al_2O_3 flake with different Miller indices under different supercooling degrees. All experiments were repeated 15 times to reduce random errors.

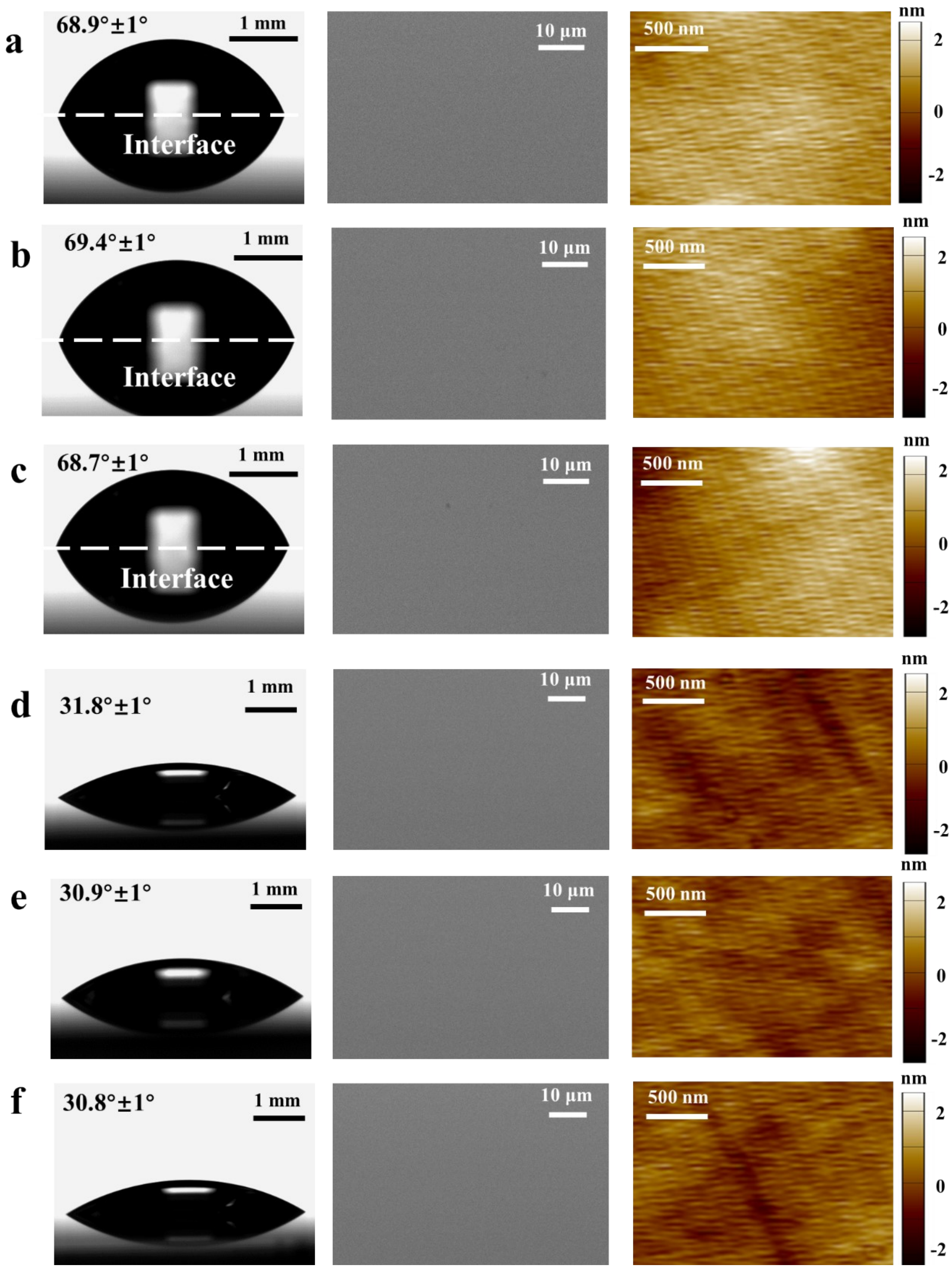

Figure S2. The contact angle, SEM and AFM of the substrates. (a) silicon wafer (100), (b) silicon wafer (110), (c) silicon wafer (111), (d) α-Al_2O_3 (A-plane), (e) α-Al_2O_3 (M-plane), (f) α-Al_2O_3 (C-plane). Figures in the first column show the contact angle of a 5 µL droplet on the substrate. Figures in the second column show the SEM image of the substrates. Figures in the third column show the AFM image of the substrates.

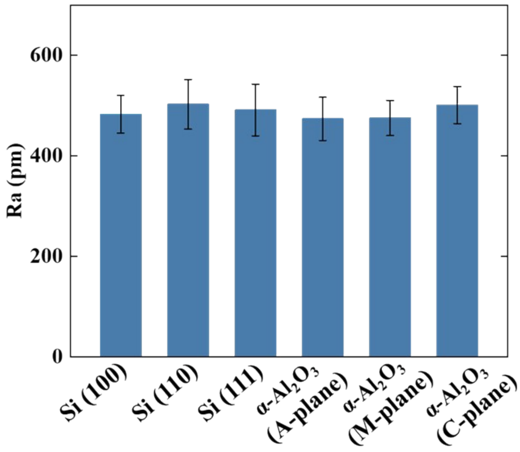

Figure S3. The surface roughness R_a of the substrates

Reference

1. D. Turnbull and B. Vonnegut, *Industrial & Engineering Chemistry*, 1952, **44**, 1292-1298.
2. M. Fitzner, G. C. Sosso, S. J. Cox and A. Michaelides, *Journal of the American Chemical Society*, 2015, **137**, 13658-13669.
3. Z. Liu, C. Li, E. C. Goonetilleke, Y. Cui and X. Huang, *The Journal of Physical Chemistry C*, 2021, **125**, 18857-18865.
4. M. Wendisch, *Journal of Atmospheric Chemistry*, 1999, **32**, 420-422.
5. A. Soni and G. N. Patey, *The Journal of Physical Chemistry C*, 2021, **125**, 10723-10737.
6. A. Goto, T. Hondoh and S. J. Mae, *Journal of Chemical Physics*, 1990, **93**, 1412-1417.
7. G. Malenkov, *Journal of Physics-Condensed Matter*, 2009, **21**.
8. E. N. Maslen, V. A. Streltsov, N. R. Streltsova, N. Ishizawa and Y. Satow, *Acta Crystallographica Section B-Structural Science*, 1993, **49**, 973-980.
9. P. Becker, P. Seyfried and H. Siegert, *Zeitschrift Fur Physik B-Condensed Matter*, 1982, **48**, 17-21.
10. R. J. Cava, F. Reidinger and B. J. Wuensch, *Solid State Communications*, 1977, **24**, 411-416.
11. L. H. Brixner, H. Y. Chen and C. M. Foris, *Journal of Solid State Chemistry*, 1981, **40**, 336-343.
12. D. A. Ksenofontov and Y. K. Kabalov, *Inorganic Materials*, 2012, **48**, 142-144.
13. D. L. Bish, *Clays and Clay Minerals*, 1993, **41**, 738-744.
14. A. Soni and G. N. Patey, *Journal of Physical Chemistry C*, 2021, **125**, 26927-26941.
15. Y. El Mendili, J. F. Bardeau, N. Randrianantoandro, F. Grasset and J. M. Greneche, *Journal of Physical Chemistry C*, 2012, **116**, 23785-23792.
16. X. Bokhimi, J. A. Toledo-Antonio, M. L. Guzman-Castillo and F. Hernandez-Beltran, *Journal of Solid State Chemistry*, 2001, **159**, 32-40.
17. A. Soni and G. N. Patey, *The Journal of Physical Chemistry C*, 2022, **126**, 6716-6723.
18. G. C. Sosso, T. Li, D. Donadio, G. A. Tribello and A. Michaelides, *The Journal of Physical Chemistry Letters*, 2016, **7**, 2350-2355.
19. A. Soni and G. N. Patey, *The Journal of Physical Chemistry C*, 2021, **125**, 26927-26941.
20. E. Chong, M. King, K. E. Marak and M. A. Freedman, *The Journal of Physical Chemistry A*, 2019, **123**, 2447-2456.
21. N. Hiranuma, N. Hoffmann, A. Kiselev, A. Dreyer, K. Zhang, G. Kulkarni, T. Koop and O. Möhler, *Atmos. Chem. Phys.*, 2014, **14**, 2315-2324.
22. Z. Zhang and X.-Y. Liu, *Chemical Society Reviews*, 2018, **47**, 7116-7139.
23. Z. Huang, S. Kaur, M. Ahmed and R. Prasher, *ACS Applied Materials & Interfaces*, 2020, **12**, 45525-45532.